Article

Chemistry & Biology

# An Analysis of MIF Structural Features that Control Functional Activation of CD74

## Graphical Abstract

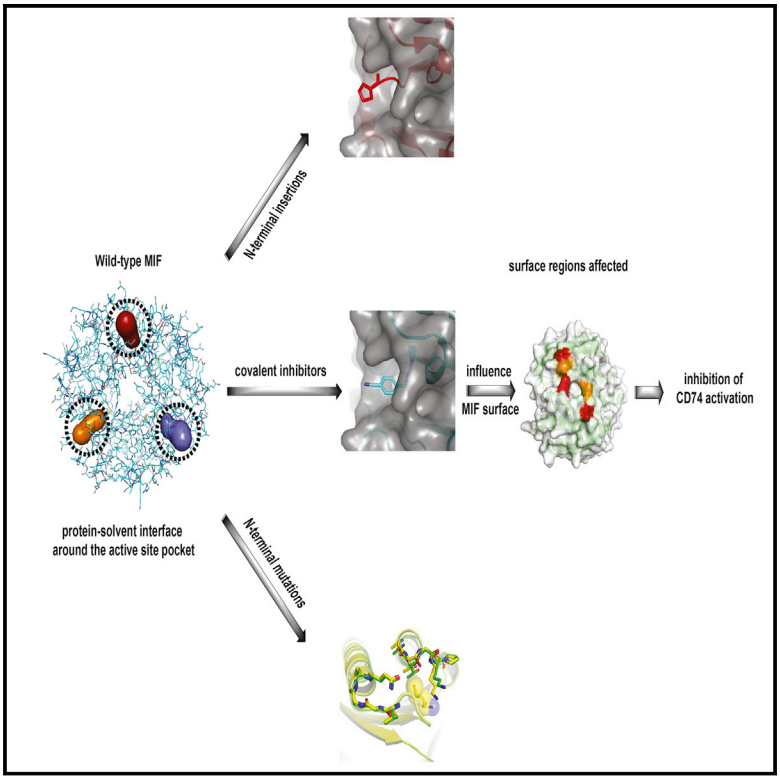


## Authors

Georgios Pantouris, Mansoor Ali Syed, Chengpeng Fan, ..., Richard Bucala, Vineet Bhandari, Elias J. Lolis

## Correspondence

elias.lolis@yale.edu

## In Brief

Pantouris et al. report the first detailed analysis of the MIF structural features that control activation of CD74. The knowledge gained by this work provides the framework for the development of potent therapeutics that block MIF-CD74 interactions.

## Highlights

- Study of the MIF structural features that control activation of CD74
- Mapping of the MIF surface residues involved in interactions with CD74
- Correlation between MIF's crystallographic B factors and CD74 activation
- Detailed analysis of the role of MIF catalytic pocket in activation of CD74

## Accession Numbers

4GRN
4GRO
4P01
4TRF
4P0H
4PLU
4PKZ
4XX7
4XX8
4TRU
5BSI
5BSC
5BS9

Pantouris et al., 2015, Chemistry & Biology 22, 1197–1205
September 17, 2015 
http://dx.doi.org/10.1016/j.chembiol.2015.08.006

Chemistry & Biology
Article

# An Analysis of MIF Structural Features that Control Functional Activation of CD74

Georgios Pantouris,[1,5] Mansoor Ali Syed,[2,5] Chengpeng Fan,[1,6] Deepa Rajasekaran,[1] Thomas Yoonsang Cho,[1,7] Eric M. Rosenberg, Jr.,[1] Richard Bucala,[3,4] Vineet Bhandari,[2] and Elias J. Lolis[1,4,*]
[1]Department of Pharmacology, Yale School of Medicine, New Haven, CT 06510, USA
[2]Department of Pediatrics, Yale School of Medicine, New Haven, CT 06510, USA
[3]Internal Medicine, Yale School of Medicine, New Haven, CT 06510, USA
[4]Yale Cancer Center, Yale School of Medicine, New Haven, CT 06510, USA
[5]Co-first author
[6]Present address: Department of Biochemistry and Molecular Biology, School of Basic Medical Sciences, Wuhan University, Wuhan 430071, China
[7]Present address: Edward A. Doisy Department of Biochemistry and Molecular Biology, St. Louis University School of Medicine, St. Louis, MO 63104, USA
*Correspondence: elias.lolis@yale.edu
http://dx.doi.org/10.1016/j.chembiol.2015.08.006

## SUMMARY

**For more than 15 years, the tautomerase active site of macrophage migration inhibitory factor (MIF) and its catalytic residue Pro1 have been being targeted for the development of therapeutics that block activation of its cell surface receptor, CD74. Neither the biological role of the MIF catalytic site nor the mechanistic details of CD74 activation are well understood. The inherently unstable structure of CD74 remains the biggest obstacle in structural studies with MIF for understanding the basis of CD74 activation. Using a novel approach, we elucidate the mechanistic details that control activation of CD74 by MIF surface residues and identify structural parameters of inhibitors that reduce CD74 biological activation. We also find that N-terminal mutants located deep in the catalytic site affect surface residues immediately outside the catalytic site, which are responsible for reduction of CD74 activation.**

## INTRODUCTION

Macrophage migration inhibitory factor (MIF) is an inflammatory protein with an eponymous activity that was first described using conditioned media of activated lymphocytes almost 50 years ago (Bloom and Bennett, 1966; David, 1966). As a cytokine, MIF has some unique properties. It is constitutively expressed with no signal sequence, is present in the cytosol of all nucleated cells where it interacts with p53 and other proteins, has an enzymatic site, possesses a solvent channel along the 3-fold axis of the trimer, and is exported to the extracellular milieu in response to diverse stimuli or cell stress (Conroy et al., 2010). MIF binds the type II receptor CD74 (Leng et al., 2003) and the chemokine receptors CXCR2 and CXCR4 (Bernhagen et al., 2007; Liehn et al., 2013), mediating distinct signaling mechanisms that lead to a variety of biological responses (Bernhagen et al., 2007; Leng et al., 2003). These activities include regulation of chemotaxis, proliferation, angiogenesis, and atherogenesis, with effects on sepsis and general inflammation, autoimmune disease, and cardiovascular disease, as well as cancer growth, survival, and metastases (Ayoub et al., 2008; Bach et al., 2008; Noels et al., 2009).

CD74 also has an intracellular role as the invariant chain associated with the processing of major histocompatibility complex (MHC) class II proteins, and is destined for proteolysis to produce a 15mer peptide (known as CLIP) that binds to the MHC class II antigen site before it is displaced by antigenic peptides (Riberdy et al., 1992). About 5% of the expressed CD74 traffics to the cell surface independent of MHC class II and functions as the MIF receptor. The recombinant CD74 extracellular domain is inherently unstable due to a number of flexible regions (Jasanoff et al., 1995, 1998), its propensity to be cleaved by enzymes (Bergmann et al., 2013; Riberdy et al., 1992), and the absence of the transmembrane region that contributes to the stability of the CD74 trimer (Ashman and Miller, 1999). Consequently, only the nuclear magnetic resonance structure of the small trimeric domain of extracellular CD74 is known (Jasanoff et al., 1998). Attempts to use the extracellular CD74 domain for structural studies with MIF have not been successful to date.

The three-dimensional structure of human MIF (Sun et al., 1996) has the same topology as two microbial enzymes that are members of the tautomerase superfamily, 4-oxalocrotonate tautomerase and 2-carboxymethyl-5-hydroxymucanate isomerase (Subramanya et al., 1996). Other than the general base catalyst, Pro1, found deep within a catalytic cavity, the proteins that belong to the tautomerase superfamily do not have significant sequence similarity. The members of this superfamily form dimers (Almrud et al., 2002), trimers (Sun et al., 1996), or hexamers (Subramanya et al., 1996) with catalytic sites at clefts between subunits, resulting in two, three, and six sites for each oligomer. All of these proteins, including MIF, have a $pK_a$ <7.0 for Pro1 (Stivers et al., 1996; Swope et al., 1998) that is three pH units lower than a typical N-terminal proline, consistent with a role as a catalytic base. A physiological substrate for MIF has not been identified, but natural (p-hydroxyphenylpyruvate) and unnatural ligands (D-dopachrome and its analogues)

were fortuitously found as "model" tautomerase substrates (Rosengren et al., 1996, 1997) and used for structure-based inhibitor design (Lubetsky et al., 1999, 2002) or high-throughput screening (Cho et al., 2011; Ouertatani-Sakouhi et al., 2010). Interestingly, the MIF-ligand complexes can function as (1) disruptors of MIF-CD74 interactions (no binding) (Cournia et al., 2009; Takahashi et al., 2009), (2) wild-type MIF (no effect on MIF binding to CD74) (Cournia et al., 2009), (3) up-regulators of CD74 binding and signaling (Jorgensen et al., 2010), or (4) CD74 antagonists (Cho et al., 2011; Jorgensen et al., 2011). The structural source of these different functional effects by ligands binding to the same site is not understood, and the parameters distinguishing these various effects remain unknown. Using MIF N-terminal mutants and MIF-covalent inhibitors, we investigated the biological role of the MIF catalytic pocket and identified mutant and ligand properties that provide new insight into the functional activation of CD74. We elucidated the surface residues that play a key role in activation of CD74, and provide the first detailed analysis of the structural features of catalytic inhibitors that dysregulate CD74 activation.

## RESULTS

### The MIF Active Site in Activation of CD74

We probed residues of the MIF enzymatic pocket involved in receptor activation by characterization of MIF mutants and MIF-covalent inhibitor complexes using a previously established lung neutrophil recruitment assay (Takahashi et al., 2009). CD74 is not expressed by neutrophils. However, intratracheal or intranasal administration of recombinant MIF activates CD74 on the surface of alveolar macrophages, leading to p44/p42 MAPK signaling and the secretion of two neutrophil-recruiting chemokines, MIP-2 and KC. There is no evidence that MIF interacts with any chemokine receptor on neutrophils, as neutrophil recruitment to the lung is inhibited by an anti-CD74 monoclonal antibody (Figure S1).

An alanine insertion mutant between Pro1 and Met2 of the MIF sequence (abbreviated as the PAM mutant) had already been structurally characterized, moving the catalytic residue Pro1 into the center of the MIF active site pocket (Lubetsky et al., 1999). In the present study two additional alanine insertions, PAAM ($PA_2M$) and PAAAM ($PA_3M$), were engineered and used with PAM to probe functional MIF-CD74 interactions. The rationale behind this approach was that the position of Pro1 was known to be at the center of the active site pocket (PAM) (Lubetsky et al., 1999), while for $PA_2M$ and $PA_3M$ Pro1 was predicted to be close to the protein-solvent interface and in the solvent, respectively. The expectation was there would be (1) no biological activity for all three mutants if a side chain from CD74 occupied the aromatic active site and was responsible for most of the binding energy, similar to a tryptophan residues for growth hormone interacting with its receptor (Clackson and Wells, 1995), (2) full biological activity for PAM, but no activity for $PA_2M$ and $PA_3M$ if the binding interactions involved surface residues at the active site-solvent boundary, or (3) full activity for all three mutants if neither the catalytic site nor the surrounding surface area were involved in CD74 interactions. The in vivo results indicate that the PAM mutant has neutrophil recruitment activity similar to that of wild-type MIF, and the $PA_2M$ and $PA_3M$ mutants have no significant activity when compared with control (Figure 1A). We also determined whether the reduction of activity was due to the inability of the $PA_2M$ and $PA_3M$ mutants to bind CD74 or whether these mutants functioned as antagonists, by administering wild-type MIF with different stoichiometries of $PA_2M$ or $PA_3M$ (Figure 1B). The results showed a dose-dependent antagonist effect for $PA_2M$ at stoichiometries of 1:1 and 1:5 (wild-type MIF/$PA_2M$). The $PA_3M$ mutant at the same stoichiometries also showed an antagonist effect but did not achieve significance between the two MIF/$PA_3M$ stoichiometries. High-resolution structures of the $PA_2M$ and $PA_3M$ mutants were determined (Table S1) to confirm the location of Pro1 (Figures 1C–1E). Based on these structures and that of wild-type MIF (PDB: 3DJH), the protein-solvent interface is in the proximity of the terminal side chain atoms for residues Lys32 and Tyr36 at the entrance of the active site pocket (Figure 1E). The mutants distinguished whether occupation of part of the catalytic site (PAM), the entire site ($PA_2M$), or extension into the solvent ($PA_3M$) results in differences for lung neutrophil recruitment due to CD74 binding and signaling.

We determined the structures of four covalent inhibitors complexed to MIF (Table S2). The electron density map of each inhibitor (**1**, **10**, **14**, and **21**) covalently bound to Pro1 and their second-order kinetics are provided in Figures 2 and 3, and the mechanism of covalent formation is shown in Figure S2. The size and orientation of each covalent inhibitor bound to Pro1 is unique, providing an alternative approach relative to the $PA_nM$ (n = 1–3) mutants to study lung neutrophil recruitment (Figures 4A–4C). We measured the recruitment of neutrophils to the lung by intranasal instillation of each MIF-inhibitor complex at a dose of 1 μg (Figure 4D). Two of the MIF-inhibitor complexes (MIF-**1** and MIF-**10**) have reduced neutrophil recruitment activity ($\leq$50%) and possess chemical moieties in the solvent or at the protein-solvent interface (Figure 4B). Covalent modification by **14** results in a small chemical adduct buried deep inside the active site (Figure 4C). The neutrophil recruitment activity of the MIF-**14** complex is similar to that of apo MIF (Figure 4D). Inhibitor **21** occupies the active site facing the channel along the 3-fold axis away from the solvent (Figure 4C) and, like **14**, has activity similar to that of wild-type MIF. The MIF-**1** and MIF-**10** complexes were further characterized and found to have a dose-dependent antagonist effect (Figure 4E).

Based on the crystallographic and in vivo results, the $PA_nM$ mutants and the covalent complexes were segregated into two groups. The first group is composed of the mutants or MIF-covalent inhibitor complexes that extend to either the MIF-solvent interface or into the solvent. These are the $PA_2M$ and $PA_3M$ mutants and the MIF-**1** and MIF-**10** complexes, which cause reduction of neutrophil recruitment to the lung. The second group (PAM mutant, MIF-**14**, and MIF-**21**) has the proline residue or inhibitors buried in the active site pocket, resulting in neutrophil-recruiting activity similar to that of wild-type MIF. These results indicate that occupancy of the catalytic site without perturbing the solvent interface does not inhibit activation of CD74 and neutrophil-recruiting activity. Any molecule that reaches the protein-solvent interface ($PA_2M$ and MIF-**10**) or extends out of the active site ($PA_3M$ and MIF-**1**) reduces MIF-mediated neutrophil-recruiting activity to lung.

 

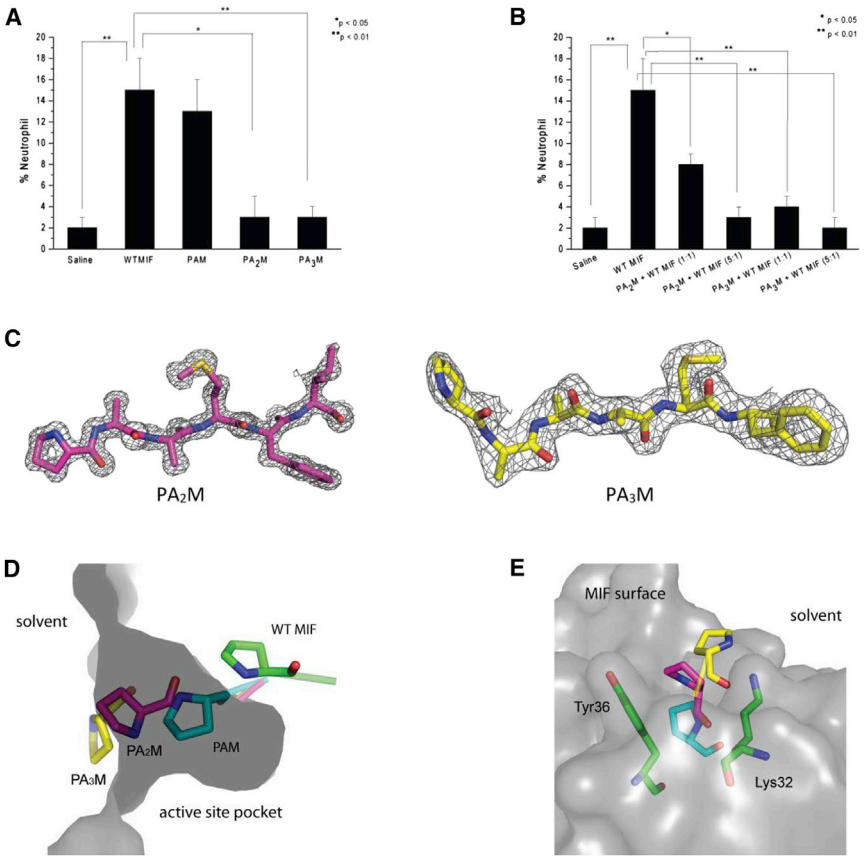


**Figure 1. In Vivo Functional Assays of $PA_nM$ Mutants and Comparison between the Position of Pro1 in the Crystal Structures of $PA_nM$ Mutants and Wild-Type MIF**

(A) In vivo neutrophil recruitment assay demonstrates that statistically significantly fewer neutrophils are recruited to the lung by $PA_2M$ and $PA_3M$, while PAM has activity similar to that of wild-type MIF.

(B) In vivo assay of wild-type MIF with the $PA_2M$ or $PA_3M$ mutant at 1:1 and 1:5 stoichiometric ratios shows antagonism by these two mutants.

(C) The $2F_o$-$F_c$ electron density maps of $PA_2M$ and $PA_3M$. The maps were contoured at 1.5σ and 1σ, respectively.

(D) Comparison of the proline positions for wild-type, PAM, $PA_2M$, and $PA_3M$ after superposition of residues 2–114 for wild-type MIF and the equivalent residues from the mutants. The gray shape represents the active-site pocket of wild-type MIF as determined by the solvent surface. The green, cyan, magenta, and yellow carbon atoms for Pro1 represent wild-type MIF, and mutants PAM, $PA_2M$, or $PA_3M$, respectively.

(E) The MIF-solvent interface at the surface of the active site is defined by the terminal side-chain atoms of the active-site residues Lys32 and Tyr36. The Pro1 position of PAM, $PA_2M$, and $PA_3M$ is shown in a different orientation relative to (D).

## Role of Pro1 and N-terminal Region in Activation of CD74

Previous studies that reported on Pro1 mutants suggested that this residue is important for MIF biological activity (Fingerle-Rowson et al., 2009; Swope et al., 1998). One of these studies showed that a Pro1 to glycine mutation (P1G) resulted in a catalytically inactive protein that maintains significant, albeit reduced, binding to its cell surface receptor CD74, and reduced biological activity (Fingerle-Rowson et al., 2009). This is in contrast to the results of the $PA_nM$ insertion mutants and the covalent inhibitors described above. We decided to probe the role of Pro1 in more detail in order to better understand the published findings. In addition to studying Pro1, we also sought answers with respect to the multiple conformations that Met2 adopts in various MIF crystal structures and whether these are related to protein function. We deleted the initiating methionine and Pro1 (ΔP1, resulting in the MIF sequence Met2-Ala114), mutated Pro1 to methionine (P1M with the mutant Met1 followed by the wild-type sequence Met2-Ala114), and created the single-site mutation Met2 to alanine (M2A). The P1M mutant had neutrophil-recruiting activity similar to that of wild-type MIF, indicating that Pro1 is not needed for activation of CD74 (Figure 5A). M2A and the deletion mutant ΔP1 reduced neutrophil recruitment activity by ~50% (Figure 5A). The three-dimensional structures were as expected for P1M and M2A (Table S3, Figure 5B). Surprisingly, one of two conformations for Met2 in the ΔP1 deletion mutant overlaps with the location of the wild-type Pro1, but this cannot be attributed to any functional activity because the M2A mutant that contains Pro1 in the wild-type location also has 50% neutrophil-recruiting activity of wild-type MIF (Figure 5B). Comparison of B factors from wild-type MIF (PDB: 3DJH) and P1G MIF (PDB: 1P1G), along with ΔP1, P1M, and M2A mutants in this study, provided some insight into their activities (Figure 5C). The last three mutants (ΔP1, M2A, and P1G) had increased B factors at the N-terminus, in contrast to the P1M mutant. Changes in the N-terminal B factors were accompanied with B-factor changes at surface-exposed residues outside the catalytic cavity. For example, all four N-terminal mutants have an increased B factor for K32, but mutation of this residue did not affect CD74 activation (Figure 5C). However, residues Tyr36 and Lys66 have a common B factor increase only for P1G, ΔP1, and M2A compared with P1M or wild-type MIF. B-Factor analysis has been used to infer the dynamics of residues or regions of proteins (Lu et al., 2006). Although the B-factor values can only be correlated qualitatively with in vivo activities, they provide insight into the structural and dynamic features of solvent-exposed residues at the cavity that lead to different neutrophil-recruiting activities. This conclusion is also supported by the findings from the previous section, which showed that chemical moieties of inhibitors or alanine insertion mutants that reach or penetrate the protein-solvent interface ($PA_2M$, $PA_3M$, MIF-**1**, and MIF-**10**) bind but do not effectively activate CD74. We mutated a number of solvent-exposed residues and tested in vivo function to glean support for this conclusion.

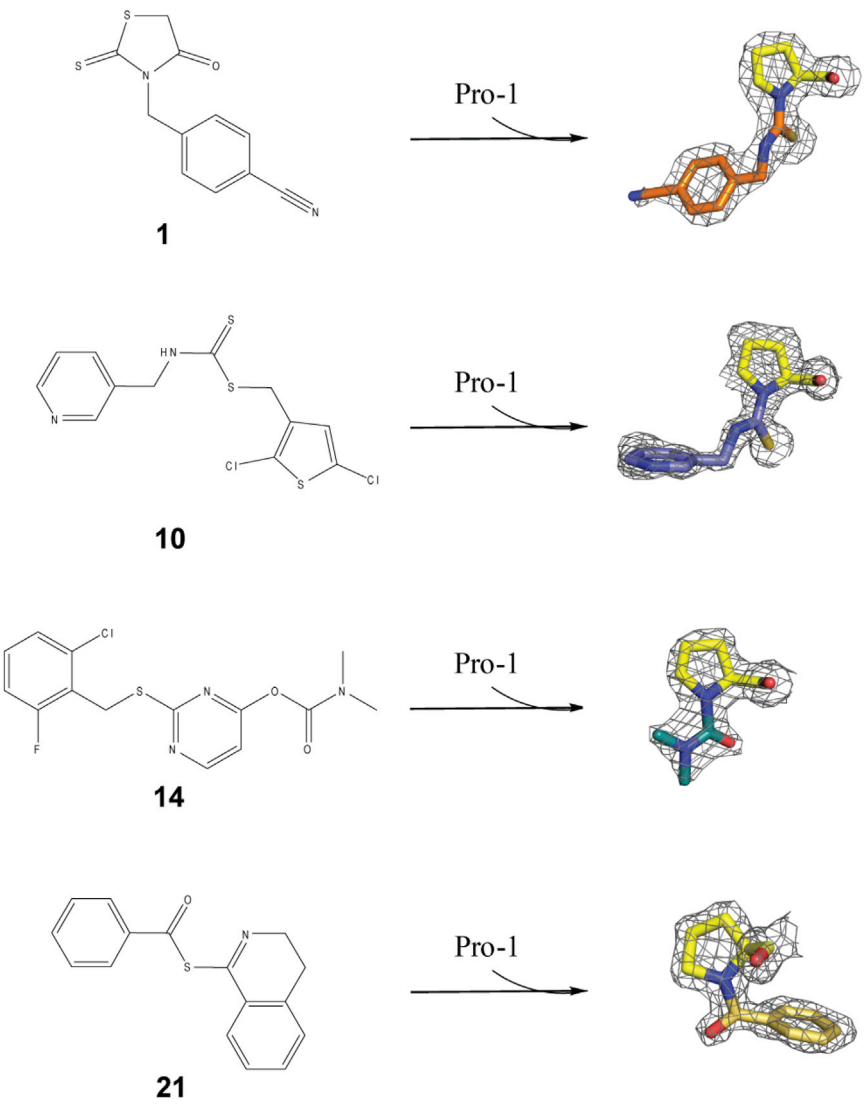


**Figure 2. Chemical Structure of Compounds 1, 10, 14, and 21 and the Electron Density of Each Pro1-Covalent Product**

Illustration of the chemical structures of compounds **1**, **10**, **14**, and **21**. The $2F_o$-$F_c$ maps of the compounds complexed to Pro1, contoured at 1.5σ, are also shown. Pro1 is shown in yellow while compounds **1**, **10**, **14**, and **21** are in orange, purple, dark green, and gold, respectively.

### MIF Surface Residues Involved in Key Interaction Points with CD74

Following the observations of the previous section, residues K32, Y36, and K66 were tested as single alanine mutants. We made a number of double mutants and tested them in vivo to identify other MIF surface residues that might interact with CD74. All the double mutants chosen for this study are located around the cavity (P34A/Q35A, S63A/I64A, and W108A/N109A) except for a control mutant (Q24A/Q25A), which is located on the surface of the first α helix away from the cavity. For the double mutants that were inactive or partially active, we made single alanine mutants to determine their activities (Figure 6A). Interestingly the alanine mutant of K32, the residue with a dramatic B-factor increase for the fully functional P1M mutant, does not affect the biological activity. P34A/Q35A and the control mutant Q24A/Q25A also maintain full activity. I64A and W108A are partially active. Y36A, K66A, and N109A do not have any neutrophil-recruiting activities. Crystallographic analyses of Y36A, K66A, N109A, and the control mutant Q24A/Q25A showed that the mutations caused no conformational changes (Table S4). Surprisingly, I64A and W108A could not be crystallized under normal MIF crystallization conditions or under new crystallization screening conditions. Therefore, we are unable to determine with certainty whether any unanticipated conformational changes are responsible for their partial activity. Nonetheless, the findings define surface regions around the active site that are involved in functional interactions with CD74 (Figure 6B).

## DISCUSSION

In the absence of an MIF-CD74 co-crystal structure, we used a novel approach to identify MIF residues that activate CD74. Alanine insertion mutants between Pro1 and Met2 as well as MIF-inhibitor complexes were employed. Neither the $PA_nM$ mutants nor the MIF-covalent inhibitor complexes can dissociate during the time course of the in vivo experiment. The use of a covalent inhibitor also prevents any off-target effects that can complicate the interpretation of the results. This allowed us to make definitive conclusions about CD74 activation. Our findings show that Pro1 and the active site pocket of MIF are not involved in interactions with CD74. These findings support the concept that a chemical moiety of an MIF inhibitor outside the active site is important for reducing MIF activation of CD74. We analyzed the surface-exposed atoms of proline for each $PA_nM$ mutant and the solvent-exposed atoms for each covalent inhibitor. We observed that the active proteins (wild-type MIF, PAM, MIF-**14**, and MIF-**21**) have a solvent-exposed surface area of atoms (either proline atoms or atoms from the covalent inhibitors) of 21 $Å^2$ or less. The partially active or inactive proteins have solvent-accessible areas of at least 44 $Å^2$ (Table S5). This is likely to be one of the physicochemical parameters that leads to CD74 antagonism.

There are three related studies that include three-dimensional structures of MIF-ligand complexes with CD74 binding or functional data in which the functional effects of chemical moieties outside the active site were not examined (Cho et al., 2011; Pantouris et al., 2014; Takahashi et al., 2009). In two of these studies, chemical moieties that penetrate into the solvent significantly reduce binding to CD74 (Cho et al., 2011; Pantouris et al.,

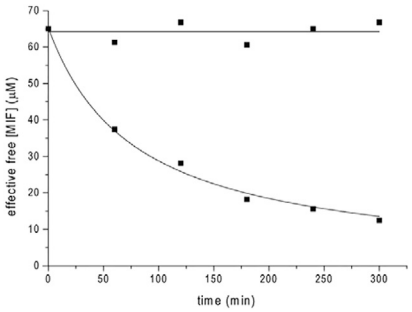


| | Second-order rate constant ($M^{-1}$ $min^{-1}$) |
|---|---|
| MIF-**1** | $1.94 \times 10^2$ |
| MIF-**10** | $1.65 \times 10^2$ |
| MIF-**14** | $2.07 \times 10^2$ |
| MIF-**21** | $1.21 \times 10^2$ |

$$[MIF] + [I] \rightarrow [MIF\text{-}I]$$

**Figure 3. Kinetic Analyses of MIF-Inhibitor Complexes**

Wild-type MIF was mixed with equal stoichiometries of **1**, **10**, **14**, and **21**, and the tautomerase activity of MIF was assessed over time. The data were fitted in a hyperbolic curve, and the second-order rate constants were calculated according to the equation $y = A/(Akt + 1)$, where $A$ is initial effective free [MIF] and $k$ is second-order rate constant. The curves were plotted in ORIGIN and are shown. The curve for only MIF-**1** is shown.

2014). In the third study, a prototypical competitive inhibitor of human MIF, (S,R)-3-(4-hydroxyphenyl)-4,5-dihydro-5-isoxazole acetic acid methyl ester (ISO-1), decreased CD74-dependent neutrophil recruitment to the lung by 50% (Takahashi et al., 2009). We analyzed the MIF-ISO-1 structure (PDB: 1LJT) and found that a chemical moiety from ISO-1 protrudes from the active site into the solvent (Figure S3) (Lubetsky et al., 2002). These findings support the concept that chemical moieties of MIF inhibitors outside the active site are important for regulating CD74 activation and signaling.

B-Factor analysis of Pro1 or Met2 mutants (P1G, P1M, and M2A), and the deletion mutant of Pro1 (ΔP1) showed differences with respect to wild-type MIF. The findings suggest that these mutants influence the dynamics of surface residues surrounding the cavity to reduce or abolish CD74 activation. Functional analyses of alanine mutants for residues identified Tyr36, Lys66, and Asn109 as key residues that control activation of CD74. Other residues, such as Lys32, Pro34, and Gln35, as well as control residues for this experiment (Gln24 and Gln25), are not involved in CD74 activation. A similar B-factor analysis has been used to directly explain the biological properties of other proteins (Hsieh et al., 2013; Marx et al., 2008).

The findings in this study reveal that neither abolishing the tautomerase activity nor mutation of Pro1 affects protein-protein

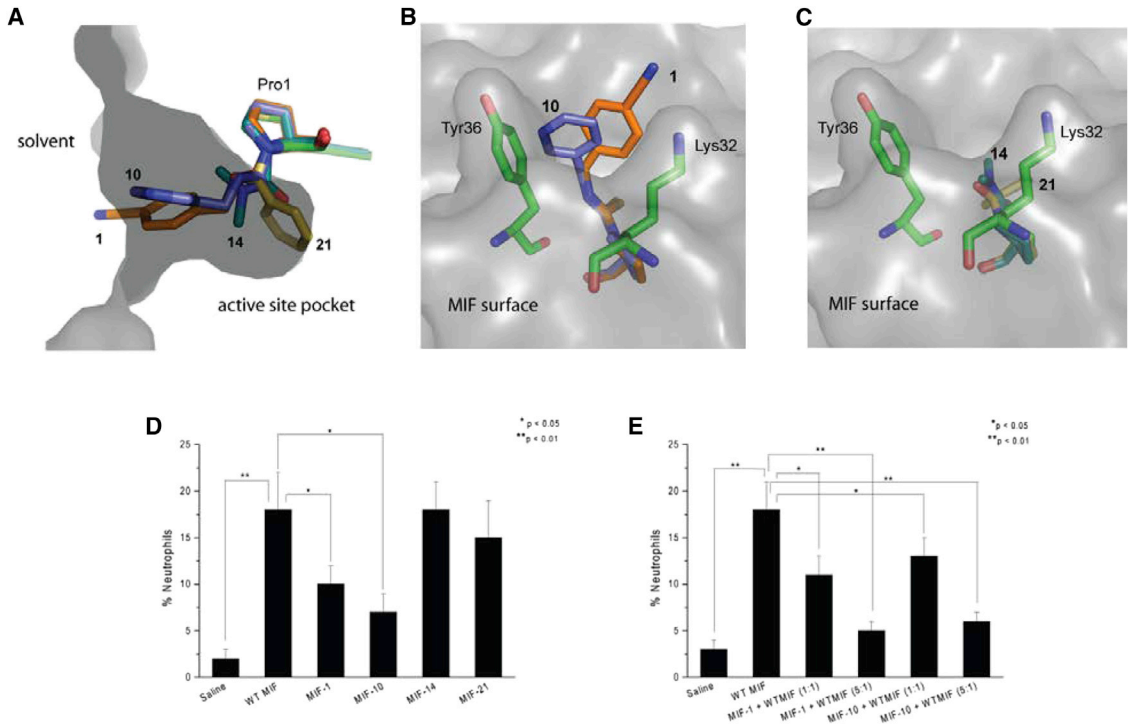


**Figure 4. Orientations of 1, 10, 14, and 21 Chemical Adducts Covalently Bonded to Pro1 and the In Vivo Functional Assay of Each Complex**

(A) The chemical adduct of **1** (orange carbon atoms) and **10** (purple carbon atoms) penetrates or is at the protein-solvent interface. Chemical adducts from **14** (dark-green carbon atoms) and **21** (gold carbon atoms) remain buried in the active-site pocket.

(B) The positions of **1** and **10** in the context of the protein-solvent interface.

(C) The positions of **14** and **21** in the context of the protein-solvent interface.

(D) Percentage neutrophils in the bronchoalveolar lavage recruited by MIF-**1**, MIF-**10**, MIF-**14**, and MIF-**21**.

(E) The two MIF-inhibitor complexes (MIF-**1** and MIF-**10**) that reduce lung neutrophil recruitment function as antagonists, based on the activity of mixtures of complexes with wild-type MIF at 1:1 and 1:5 stoichiometric ratios, respectively.

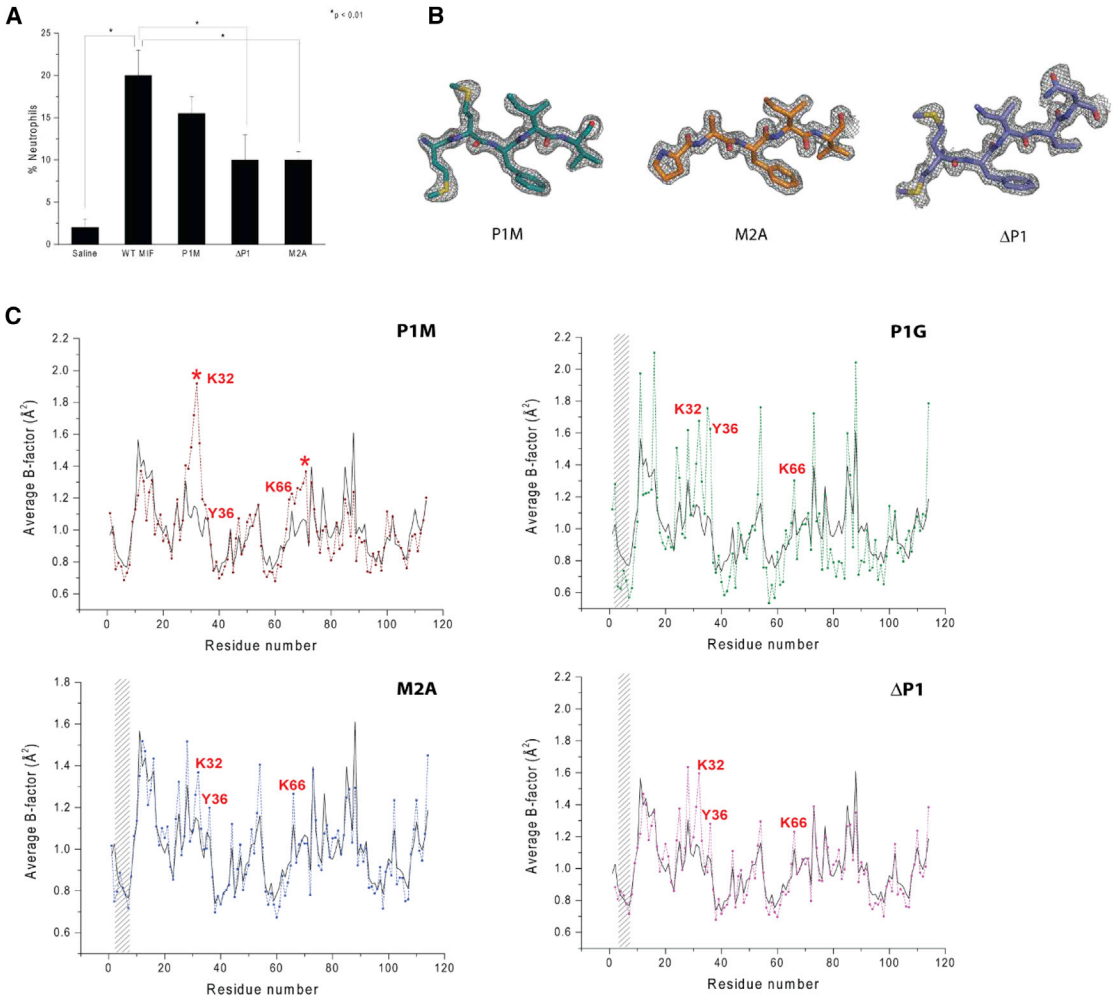


**Figure 5. Neutrophil Recruitment Assay and Crystallographic B-Factor Analyses of MIF N-Terminal Mutants**

(A) In vivo neutrophil recruitment assay of P1M, ΔP1, and M2A. The ΔP1 and M2A inhibit recruitment of neutrophil to the lung by ~50%. The reduction of P1M was not statistically significant.

(B) The $2F_o$-$F_c$ electron density maps of P1M, M2A, and ΔP1 mutants. The maps were contoured at 1.5σ.

(C) Analyses of the residual crystallographic B factors of P1M, P1G, M2A, and ΔP1. Mutation of P1M increased the normalized B factors in two particular regions outside the active site. These regions are marked with a star. The P1G, M2A, and ΔP1 mutants increase the B factors of the highlighted N-terminal part of the β1 strand, resulting in changes that eventually reach the surface.

interactions and reduction of CD74 activation. The mutants of Pro1 (and Met2) influence the B factors of specific surface residues that reduce CD74 activation when mutated, indicating that residues at the surface surrounding the catalytic site pocket of MIF are involved in activation of CD74. The mechanism for the N-terminal mutants that leads to B-factor changes at specific surface residues remains to be determined by molecular dynamics simulations. The knowledge gained herein advances our understanding of the structural and chemical basis of CD74 activation and provides vital information for the development of new MIF-based therapeutics.

## SIGNIFICANCE

**Macrophage MIF is a cytokine that is expressed in all types of human cells and plays a key role in many diseases via its binding to the cell surface receptor CD74. A small-molecule inhibitor of CD74 is yet to be discovered, while there are numerous tautomerase inhibitors of MIF. The MIF-inhibitor complexes have varying effects in their interactions with CD74 including abolishing interactions, up-regulating CD74 signaling, and antagonizing CD74 signaling, or have no effect on CD74 function. Our study provides the first comprehensive analysis of the MIF parameters that control functional activation of CD74, and clarifies the properties of MIF inhibitors that effectively inhibit CD74. First, the catalytic pocket of MIF is not involved in interactions with CD74. However, inhibitors that bind to the pocket must penetrate the protein-solvent interface to function as CD74 antagonists. Second, mutations of N-terminal residues affect key surface residues that cause reduction or complete inhibition of CD74 activation when mutated. These key residues are**

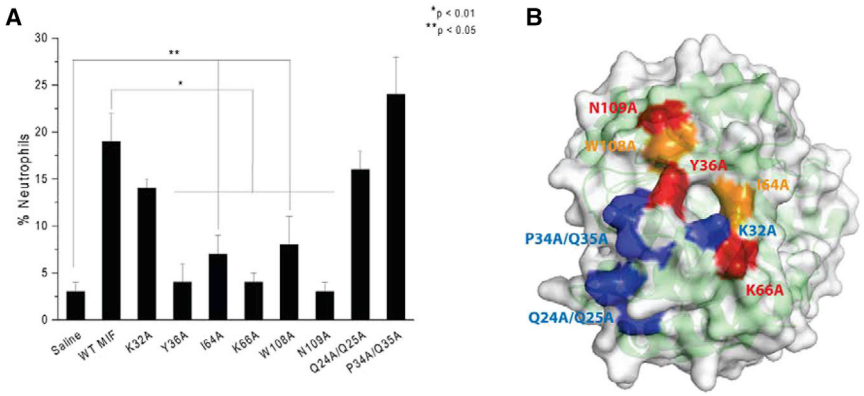


**Figure 6. Surface Mutations Reveal the MIF Residues that Play a Key Role in Activation of CD74**

(A) Neutrophil recruitment activities of the surface mutants. The effect of Y36A, K66A, and N109 are not statistically significant compared with saline alone ($p > 0.05$). The partial agonists I64A and W108A are statistically significant compared with MIF ($p < 0.01$) and saline ($p < 0.05$).

(B) The MIF surface mutants used in this study are shown in different colors according to their in vivo activities and crystallographic structures. The red highlighted regions show the surface residues that do not activate CD74 with a three-dimensional structure illustrating that there are no conformational changes. Orange denotes the two partial agonists that could not be crystallized. The fully active surface residues are shown in blue.

**mapped on the three-dimensional surface of MIF to identify the region involved in CD74 interactions. Mutants of residues that do not affect CD74 activation are also used to provide a more comprehensive map for understanding these interactions. This study enhances our understanding of MIF-mediated CD74 activation and aids in the development of novel therapeutics.**

## EXPERIMENTAL PROCEDURES

### Mutagenesis

The MIF mutants were synthesized using the megaprimer method (Ke and Madison, 1997). The pET-11b/WT MIF served as the template, and the oligonucleotides shown in the Supplemental Information were amplified, producing the desired mutation. The clone of PAM was previously reported (Lubetsky et al., 1999).

### Expression and Purification of Recombinant Human MIF and MIF Mutants

Expression and purification of recombinant human MIF and MIF mutants were performed as described previously (Lubetsky et al., 1999). Each pET-11b plasmid containing the cDNA of interest was transformed in *Escherichia coli* BL21-Gold (DE3) cells. The cells were grown at 37°C to an $OD_{600}$ of 0.6 and induced using isopropyl β-D-1-thiogalactopyranoside at final concentration of 1 mM. After 4 hr at 37°C, the cells were harvested and stored at −20°C until further use. For purification, the cells were thawed and lysed using sonication in 20 mM Tris (pH 7.4) and 20 mM NaCl containing a protease inhibitor cocktail tablet. Cell debris was removed via centrifugation for 45 min at 28,000 × *g*. The supernatant was filtered using a syringe-driven filter unit and loaded onto a Q-Sepharose column (120 ml) connected in series with an SP column (55 ml). Both wild-type MIF and MIF mutants were not retained from either columns and were collected as flow-though, which was ~95% pure. MIF was further purified using size-exclusion chromatography (16/60 Superdex 75) in the same buffer.

### Enzyme Kinetics

Kinetic analyses of MIF-covalent inhibitor formation were performed using the Tecan Infinite M200 spectrophotometer at 306 nm with a Corning semitransparent 96-well plate. Prior to carrying out any experiment, a stock solution of 4-hydroxyphenylpyruvate (4-HPP) in 0.5 M ammonium acetate (pH 6.2) was prepared and equilibrated for 24 hr at room temperature to allow for keto-enol equilibration. MIF and each inhibitor were mixed, and an aliquot was removed at various time points and added to wells containing the tautomerase mixture to measure the remaining tautomerase activity. Each measurement lasted 90 s with readings taken every 10 s. The volume of the tautomerase reaction mixture was 150 μl and contained 0.416 M borate (pH 6.2), 0.5 mM HPP, DMSO or inhibitor dissolved in DMSO, and 5 μM MIF. The final concentration of **1**, **10**, **14**, and **21** was 5 μM (equal stoichiometric ratios with MIF). In all cases, controls and compounds were at a final concentration of 1% (v/v) DMSO. All experiments were performed at 25°C. The data were fitted to a hyperbolic curve using ORIGIN 9.0, and the second-order rate constants were calculated as described elsewhere (Crichlow et al., 2012).

### Murine In Vivo Recruitment of Neutrophils to the Lung

Neutrophil recruitment was measured using C57BL/6J mice (8–12 weeks old) according to the protocol described by Fan et al. (2013). All samples were administrated to murine lungs via the intranasal route as 50-μl saline solutions with recombinant human MIF at 1 μg, and the anti-murine CD74 monoclonal antibody (BD Pharmingen, cat. #555317) at 10 μg. MIF mutants and each of the MIF-covalent inhibitor complexes were also administrated as solutions containing 1 μg of sample. Each compound was incubated with MIF at 1:1 stoichiometric ratio at 4°C for 24 hr. The complete modification of MIF by each inhibitor at 24 hr was based on the second-order kinetics of each inhibitor. For in vivo antagonist assays, wild-type MIF and each mutant or MIF-inhibitor complex were administered at 1:1 and 1:5 stoichiometric ratios (wild-type MIF/MIF mutant or MIF-inhibitor complex). The total number of neutrophils was calculated using the differential cell count of a minimum number of 200 cells stained with HEMA 3 (Fisher Scientific). For direct comparison of two datasets the two-tailed t test was used. The protocol followed for the mouse experiments was reviewed and approved by the Yale University Institutional Animal Care and Use Committee.

### Crystallization, Data Collection, Structure Determination, and Refinement

The MIF mutants and MIF-covalent inhibitor complexes were crystallized by vapor diffusion in hanging-drop trays. Purified MIF mutants were concentrated to 18 mg/ml. For the MIF-covalent inhibitor complexes, MIF was concentrated to 18 mg/ml, mixed with each compound at 1:3 M ratio (MIF/inhibitor), and incubated at 4°C overnight. Before crystallization, all samples were spun for 5 min at 16,000 × *g*. Equal volumes of mutant or MIF-inhibitor complex were mixed with the well reservoir (2 μl:2 μl) and allowed to equilibrate at 20°C. Crystals appeared within 2 weeks. $PA_2M$ and $PA_3M$ were crystallized in 20 mM 2-(N-morpholino)ethanesulfonic acid (pH 6.5) and 2 M ammonium sulfate. The other mutants and the four MIF-inhibitor complexes were crystallized in 20 mM Tris (pH 7.4), 2 M ammonium sulfate, and 3% 2-propanol. All crystals were flash-frozen in the mother liquor with 25% glycerol. Diffraction data of $PA_2M$ were collected at beamline X25 (wavelength = 1.1 Å) of the Brookhaven National Synchrotron Light Source. Diffraction data of $PA_3M$, P1M, Q24A/Q25A, and the MIF-covalent inhibitor complexes were collected at Yale School of Medicine on an R-AXIS IV++ image plate detector (Rigaku) with a Rigaku 007 rotating copper anode X-ray generator (wavelength = 1.5418 Å). Diffraction data of Y36A, K66A, and N109A were also collected at Yale School of Medicine on a Rigaku Pilatus 200K Detector using the same type of generator described above. For M2A and ΔP1, the diffraction data were collected at St. Louis University School of Medicine, using an R-AXIS IV++ image plate

detector, wavelength = 1.5418 Å. All datasets were collected at temperatures between 90 and 100 K. All datasets (except $PA_3M$) were integrated and scaled using HKL2000 programs suite (Otwinowski and Minor, 1997). For $PA_3M$, the dataset was integrated with MOSFLM (Battye et al., 2011) and scaled with SCALA (Evans, 2006). The structures were solved by molecular replacement using PHASER (McCoy et al., 2007) and refined by PHENIX (Adams et al., 2010) ($PA_2M$ and $PA_3M$) or REFMAC (Winn et al., 2003) (for the other mutants and MIF-covalent inhibitor complexes). Ramachandran analysis showed 0% outliers and 98.20% (P1M), 98.81% (M2A), 98.79% (ΔP1), 98.88% ($PA_2M$), 97.72% ($PA_3M$), 98.81% (Q24A/Q25A), 98.33% (Y36A), 98.81% (K66A), 97.92% (N109A), 98.51% (MIF-**1**), 99.09% (MIF-**10**), 99.11% (MIF-**14**), and 98.21% (MIF-**21**) residues in preferred regions. Topology models of the inhibitors were produced by the PRODRG server (Schuttelkopf and van Aalten, 2004) and fitted in the model using Coot (Emsley et al., 2010). The $2F_o$-$F_c$ maps were generated by FFT (Winn et al., 2011) and visualized in PyMOL (DeLano, 2002). The structure of wild-type MIF (PDB: 3DJH) was superposed onto the MIF mutants and MIF-inhibitor complexes using SUPERPOSE (CCP4 supported) (Winn et al., 2011). The root-mean-square deviation values showed high superposition agreement with wild-type MIF. The values varied between 0.10 and 0.29 Å and are provided in Table S6. Analyses of the solvent-accessible surface area of atoms in MIF-inhibitor complexes or the proline in wild-type and $PA_nM$ mutants were calculated using AREAIMOL (Winn et al., 2011). The detailed statistics of the datasets are presented in Table S1 ($PA_2M$ and $PA_3M$), Table S2 (MIF-covalent inhibitor complexes), Table S3 (P1M, M2A and ΔP1), and Table S4 (Q24A/Q25A, Y36A, K66A and N109A).

## ACCESSION NUMBERS

Coordinates and structural factors have been deposited in the PDB under the accession codes PDB: 4GRN ($PA_2M$), 4GRO ($PA_3M$), 4P01 (MIF-**1**), 4TRF (MIF-**10**), 4P0H (MIF-**14**), 4PLU (MIF-**21**), 4PKZ (P1M), 4XX7 (M2A), 4XX8 (ΔP1), 4TRU (Q24A/Q25A), 5BSI (Y36A), 5BSC (K66A), and 5BS9 (N109A).

## SUPPLEMENTAL INFORMATION

Supplemental Information includes three figures, six tables, and a list of the primers used in this study and can be found with this article online at http://dx.doi.org/10.1016/j.chembiol.2015.08.006.

## AUTHOR CONTRIBUTIONS

G.P. designed the strategy that was followed in the experiments, expressed and purified wild-type MIF and all the MIF mutants, supervised the kinetic experiments, analyzed data, performed the crystallization of the MIF mutants and MIF-inhibitor complexes, carried out the in vivo studies of I64A, W108A, and N109A, and wrote the manuscript. M.A.S. carried out the majority of the in vivo studies ($PA_nM$ mutants, MIF-inhibitor complexes, N-terminal mutants and surface mutants) and analyzed data. C.F. solved the structures of $PA_2M$ and $PA_3M$ mutants. D.R. contributed to the biochemistry. T.Y.C. carried out the high-throughput screening of small-molecule inhibitors. E.R. performed the kinetics experiments for MIF-inhibitor complexes. R.B. contributed to data analysis. V.B. supervised the in vivo studies. E.J.L. conceived and supervised the project, analyzed data, and wrote the manuscript. All authors have given approval for the final version of the manuscript.

## ACKNOWLEDGMENTS

We thank Dr. Sorabh Agarwal, Saint Louis University School of Medicine, for collecting the data sets of M2A and ΔP1 mutants. This work was supported by NIH grants AI065029 and AI082295.

Received: March 16, 2015
Revised: July 19, 2015
Accepted: August 10, 2015
Published: September 10, 2015

## REFERENCES

Adams, P.D., Afonine, P.V., Bunkoczi, G., Chen, V.B., Davis, I.W., Echols, N., Headd, J.J., Hung, L.W., Kapral, G.J., Grosse-Kunstleve, R.W., et al. (2010). PHENIX: a comprehensive Python-based system for macromolecular structure solution. Acta Crystallogr. D Biol. Crystallogr. *66*, 213–221.

Almrud, J.J., Kern, A.D., Wang, S.C., Czerwinski, R.M., Johnson, W.H., Murzin, A.G., Hackert, M.L., and Whitman, C.P. (2002). The crystal structure of YdcE, a 4-oxalocrotonate tautomerase homologue from *Escherichia coli*, confirms the structural basis for oligomer diversity. Biochemistry *41*, 12010–12024.

Ashman, J.B., and Miller, J. (1999). A role for the transmembrane domain in the trimerization of the MHC class II-associated invariant chain. J. Immunol. *163*, 2704–2712.

Ayoub, S., Hickey, M.J., and Morand, E.F. (2008). Mechanisms of disease: macrophage migration inhibitory factor in SLE, RA and atherosclerosis. Nat. Clin. Pract. Rheum. *4*, 98–105.

Bach, J.P., Rinn, B., Meyer, B., Dodel, R., and Bacher, M. (2008). Role of MIF in inflammation and tumorigenesis. Oncology *75*, 127–133.

Battye, T.G., Kontogiannis, L., Johnson, O., Powell, H.R., and Leslie, A.G. (2011). iMOSFLM: a new graphical interface for diffraction-image processing with MOSFLM. Acta Crystallogr. D Biol. Crystallogr. *67*, 271–281.

Bergmann, H., Yabas, M., Short, A., Miosge, L., Barthel, N., Teh, C.E., Roots, C.M., Bull, K.R., Jeelall, Y., Horikawa, K., et al. (2013). B cell survival, surface BCR and BAFFR expression, CD74 metabolism, and CD8- dendritic cells require the intramembrane endopeptidase SPPL2A. J. Exp. Med. *210*, 31–40.

Bernhagen, J., Krohn, R., Lue, H., Gregory, J.L., Zernecke, A., Koenen, R.R., Dewor, M., Georgiev, I., Schober, A., Leng, L., et al. (2007). MIF is a noncognate ligand of CXC chemokine receptors in inflammatory and atherogenic cell recruitment. Nat. Med. *13*, 587–596.

Bloom, B.R., and Bennett, B. (1966). Mechanism of a reaction in vitro associated with delayed-type hypersensitivity. Science *153*, 80–82.

Cho, Y., Vermeire, J.J., Merkel, J.S., Leng, L., Du, X., Bucala, R., Cappello, M., and Lolis, E. (2011). Drug repositioning and pharmacophore identification in the discovery of hookworm MIF inhibitors. Chem. Biol. *18*, 1089–1101.

Clackson, T., and Wells, J.A. (1995). A hot spot of binding energy in a hormone-receptor interface. Science *267*, 383–386.

Conroy, H., Mawhinney, L., and Donnelly, S.C. (2010). Inflammation and cancer: macrophage migration inhibitory factor (MIF)—the potential missing link. QJM *103*, 831–836.

Cournia, Z., Leng, L., Gandavadi, S., Du, X., Bucala, R., and Jorgensen, W.L. (2009). Discovery of human macrophage migration inhibitory factor (MIF)-CD74 antagonists via virtual screening. J. Med. Chem. *52*, 416–424.

Crichlow, G.V., Fan, C., Keeler, C., Hodsdon, M., and Lolis, E.J. (2012). Structural interactions dictate the kinetics of macrophage migration inhibitory factor inhibition by different cancer-preventive isothiocyanates. Biochemistry *51*, 7506–7514.

David, J.R. (1966). Delayed hypersensitivity in vitro: its mediation by cell-free substances formed by lymphoid cell-antigen interaction. Proc. Natl. Acad. Sci. USA *56*, 72–77.

DeLano, W.L. (2002). The PyMOL Molecular Graphics System (DeLano Scientific).

Emsley, P., Lohkamp, B., Scott, W.G., and Cowtan, K. (2010). Features and development of Coot. Acta Crystallogr. D Biol. Crystallogr. *66*, 486–501.

Evans, P. (2006). Scaling and assessment of data quality. Acta Crystallogr. D Biol. Crystallogr. *62*, 72–82.

Fan, C., Rajasekaran, D., Syed, M.A., Leng, L., Loria, J.P., Bhandari, V., Bucala, R., and Lolis, E.J. (2013). MIF intersubunit disulfide mutant antagonist supports activation of CD74 by endogenous MIF trimer at physiologic concentrations. Proc. Natl. Acad. Sci. USA *110*, 10949.

Fingerle-Rowson, G., Kaleswarapu, D.R., Schlander, C., Kabgani, N., Brocks, T., Reinart, N., Busch, R., Schutz, A., Lue, H., Du, X., et al. (2009). A tautomerase-null MIF gene knock-in mouse reveals that protein interactions and not

 

enzymatic activity mediate MIF-dependent growth regulation. Mol. Cell. Biol. *29*, 1922–1932.

Hsieh, Y.C., Chia, T.S., Fun, H.K., and Chen, C.J. (2013). Crystal structure of dimeric flavodoxin from *Desulfovibrio gigas* suggests a potential binding region for the electron-transferring partner. Int. J. Mol. Sci. *14*, 1667–1683.

Jasanoff, A., Park, S.J., and Wiley, D.C. (1995). Direct observation of disordered regions in the major histocompatibility complex class II-associated invariant chain. Proc. Natl. Acad. Sci. USA *92*, 9900–9904.

Jasanoff, A., Wagner, G., and Wiley, D.C. (1998). Structure of a trimeric domain of the MHC class II-associated chaperonin and targeting protein Ii. EMBO J. *17*, 6812–6818.

Jorgensen, W.L., Gandavadi, S., Du, X., Hare, A.A., Trofimov, A., Leng, L., and Bucala, R. (2010). Receptor agonists of macrophage migration inhibitory factor. Bioorg. Med. Chem. Lett. *20*, 7033–7036.

Jorgensen, W.L., Trofimov, A., Du, X., Hare, A.A., Leng, L., and Bucala, R. (2011). Benzisothiazolones as modulators of macrophage migration inhibitory factor. Bioorg. Med. Chem. Lett. *21*, 4545–4549.

Ke, S.H., and Madison, E.L. (1997). Rapid and efficient site-directed mutagenesis by single-tube 'megaprimer' PCR method. Nucleic Acids Res. *25*, 3371–3372.

Leng, L., Metz, C.N., Fang, Y., Xu, J., Donnelly, S., Baugh, J., Delohery, T., Chen, Y., Mitchell, R.A., and Bucala, R. (2003). MIF signal transduction initiated by binding to CD74. J. Exp. Med. *197*, 1467–1476.

Liehn, E.A., Kanzler, I., Konschalla, S., Kroh, A., Simsekyilmaz, S., Sonmez, T.T., Bucala, R., Bernhagen, J., and Weber, C. (2013). Compartmentalized protective and detrimental effects of endogenous macrophage migration-inhibitory factor mediated by CXCR2 in a mouse model of myocardial ischemia/reperfusion. Arterioscler. Thromb. Vasc. Biol. *33*, 2180–2186.

Lu, W.C., Wang, C.Z., Yu, E.W., and Ho, K.M. (2006). Dynamics of the trimeric AcrB transporter protein inferred from a B-factor analysis of the crystal structure. Proteins *62*, 152–158.

Lubetsky, J.B., Swope, M., Dealwis, C., Blake, P., and Lolis, E. (1999). Pro-1 of macrophage migration inhibitory factor functions as a catalytic base in the phenylpyruvate tautomerase activity. Biochemistry *38*, 7346–7354.

Lubetsky, J.B., Dios, A., Han, J., Aljabari, B., Ruzsicska, B., Mitchell, R., Lolis, E., and Al-Abed, Y. (2002). The tautomerase active site of macrophage migration inhibitory factor is a potential target for discovery of novel anti-inflammatory agents. J. Biol. Chem. *277*, 24976–24982.

Marx, P.F., Brondijk, T.H., Plug, T., Romijn, R.A., Hemrika, W., Meijers, J.C., and Huizinga, E.G. (2008). Crystal structures of TAFI elucidate the inactivation mechanism of activated TAFI: a novel mechanism for enzyme autoregulation. Blood *112*, 2803–2809.

McCoy, A.J., Grosse-Kunstleve, R.W., Adams, P.D., Winn, M.D., Storoni, L.C., and Read, R.J. (2007). Phaser crystallographic software. J. Appl. Crystallogr. *40*, 658–674.

Noels, H., Bernhagen, J., and Weber, C. (2009). Macrophage migration inhibitory factor: a noncanonical chemokine important in atherosclerosis. Trends Cardiovasc. Med. *19*, 76–86.

Otwinowski, Z., and Minor, W. (1997). Processing of x-ray diffraction data collected in oscillation mode. Methods Enzymol. *276*, 307–325.

Ouertatani-Sakouhi, H., Liu, M., El-Turk, F., Cuny, G.D., Glicksman, M.A., and Lashuel, H.A. (2010). Kinetic-based high-throughput screening assay to discover novel classes of macrophage migration inhibitory factor inhibitors. J. Biomol. Screen *15*, 347–358.

Pantouris, G., Rajasekaran, D., Garcia, A.B., Ruiz, V.G., Leng, L., Jorgensen, W.L., Bucala, R., and Lolis, E.J. (2014). Crystallographic and receptor binding characterization of Plasmodium falciparum macrophage migration inhibitory factor complexed to two potent inhibitors. J. Med. Chem. *57*, 8652–8656.

Riberdy, J.M., Newcomb, J.R., Surman, M.J., Barbosa, J.A., and Cresswell, P. (1992). HLA-DR molecules from an antigen-processing mutant cell line are associated with invariant chain peptides. Nature *360*, 474–477.

Rosengren, E., Bucala, R., Aman, P., Jacobsson, L., Odh, G., Metz, C.N., and Rorsman, H. (1996). The immunoregulatory mediator macrophage migration inhibitory factor (MIF) catalyzes a tautomerization reaction. Mol. Med. *2*, 143–149.

Rosengren, E., Aman, P., Thelin, S., Hansson, C., Ahlfors, S., Bjork, P., Jacobsson, L., and Rorsman, H. (1997). The macrophage migration inhibitory factor MIF is a phenylpyruvate tautomerase. FEBS Lett. *417*, 85–88.

Schuttelkopf, A.W., and van Aalten, D.M.F. (2004). PRODRG: a tool for high-throughput crystallography of protein-ligand complexes. Acta Crystallogr. D Biol. Crystallogr. *60*, 1355–1363.

Stivers, J.T., Abeygunawardana, C., and Mildvan, A.S. (1996). 15N NMR relaxation studies of free and inhibitor-bound 4-oxalocrotonate tautomerase: backbone dynamics and entropy changes of an enzyme upon inhibitor binding. Biochemistry *35*, 16036–16047.

Subramanya, H.S., Roper, D.I., Dauter, Z., Dodson, E.J., Davies, G.J., Wilson, K.S., and Wigley, D.B. (1996). Enzymatic ketonization of 2-hydroxymuconate: specificity and mechanism investigated by the crystal structures of two isomerases. Biochemistry *35*, 792–802.

Sun, H.W., Bernhagen, J., Bucala, R., and Lolis, E. (1996). Crystal structure at 2.6-A resolution of human macrophage migration inhibitory factor. Proc. Natl. Acad. Sci. USA *93*, 5191–5196.

Swope, M., Sun, H.W., Blake, P.R., and Lolis, E. (1998). Direct link between cytokine activity and a catalytic site for macrophage migration inhibitory factor. EMBO J. *17*, 3534–3541.

Takahashi, K., Koga, K., Linge, H.M., Zhang, Y., Lin, X., Metz, C.N., Al-Abed, Y., Ojamaa, K., and Miller, E.J. (2009). Macrophage CD74 contributes to MIF-induced pulmonary inflammation. Respir. Res. *10*, 33.

Winn, M.D., Murshudov, G.N., and Papiz, M.Z. (2003). Macromolecular TLS refinement in REFMAC at moderate resolutions. Methods Enzymol. *374*, 300–321.

Winn, M.D., Ballard, C.C., Cowtan, K.D., Dodson, E.J., Emsley, P., Evans, P.R., Keegan, R.M., Krissinel, E.B., Leslie, A.G., McCoy, A., et al. (2011). Overview of the CCP4 suite and current developments. Acta Crystallogr. D Biol. Crystallogr. *67*, 235–242.